The Journal of Chemical Physics

Observations of Dicke narrowing and speed dependence in air-broadened CO_2 lineshapes near 2.06 μm

Cite as: J. Chem. Phys. **141**, 174301 (2014); https://doi.org/10.1063/1.4900502
Submitted: 11 August 2014 . Accepted: 15 October 2014 . Published Online: 03 November 2014

Thinh Q. Bui, David A. Long, Agata Cygan, Vincent T. Sironneau, Daniel W. Hogan, Priyanka M. Rupasinghe, Roman Ciuryło, Daniel Lisak, and Mitchio Okumura

THE JOURNAL OF CHEMICAL PHYSICS **141**, 174301 (2014)

Observations of Dicke narrowing and speed dependence in air-broadened CO_2 lineshapes near 2.06 μm

Thinh Q. Bui,[1,a)] David A. Long,[2,a)] Agata Cygan,[3,a)] Vincent T. Sironneau,[2] Daniel W. Hogan,[1] Priyanka M. Rupasinghe,[1] Roman Ciuryło,[3] Daniel Lisak,[3] and Mitchio Okumura[1,a)]

[1]*Division of Chemistry and Chemical Engineering, California Institute of Technology, Pasadena, California 91125, USA*
[2]*Material Measurement Laboratory, National Institute of Standards and Technology, 100 Bureau Drive, Gaithersburg, Maryland 20899, USA*
[3]*Institute of Physics, Faculty of Physics, Astronomy, and Informatics, Nicolaus Copernicus University, Grudziadzka 5, 87-100 Torun, Poland*

(Received 11 August 2014; accepted 15 October 2014; published online 3 November 2014)

Frequency-stabilized cavity ring-down spectroscopy was used to study CO_2 lineshapes in the (20013) ← (00001) band centered near 2.06 μm. Two rovibrational transitions were chosen for this study to measure non-Voigt collisional effects for air-broadened lines over the pressure range of 7 kPa–28 kPa. Lineshape analysis for both lines revealed evidence of simultaneous Dicke (collisional) narrowing and speed-dependent effects that would introduce biases exceeding 2% in the retrieved air-broadening parameters if not incorporated in the modeling of CO_2 lineshapes. Additionally, correlations between velocity- and phase/state changing collisions greatly reduced the observed Dicke narrowing effect. As a result, it was concluded that the most appropriate line profile for modeling CO_2 lineshapes near 2.06 μm was the correlated speed-dependent Nelkin-Ghatak profile, which includes all of the physical effects mentioned above and leads to a consistent set of line shape parameters that are linear with gas pressure. © *2014 AIP Publishing LLC*. [http://dx.doi.org/10.1063/1.4900502]

INTRODUCTION

Current and upcoming remote sensing missions (including NASA's OCO-2 and ASCENDS) have necessitated high-precision studies to retrieve accurate lineshape parameters in the $4\nu_2 + \nu_3$ band [(20013) ← (00001)] centered at 2.06 μm.[1–3] The (20013) ← (00001) band, along with two other bands, (20012) ← (00001) and (20011) ← (00001), form the Fermi triad of CO_2 bands spanning 4700–5200 cm^{-1}. Since these missions have set a target precision of 0.25%, we studied non-Voigt lineshape effects to achieve a reduction in uncertainties of the retrieved spectroscopic parameters to below the 1% limit of the Voigt profile (VP).[4]

It is well established from high resolution molecular spectroscopy that the Voigt profile is inadequate to properly describe high-precision measurements of CO_2 lineshapes.[5–13] Recently, Casa *et al.*[10] used laser absorption spectroscopy to measure CO_2 lineshapes of the $\nu_1 + 2\nu_2 + \nu_3$ band [(20012) ← (00001)] at 2.0 μm. By recording spectra with high resolution (≈1 MHz) and high signal-to-noise ratios (≈10000:1), they were able to resolve non-Voigt features. However, the line profiles employed in their analysis – Voigt, Galatry, Nelkin-Ghatak, speed-dependent Voigt, correlated Galatry and Nelkin-Ghatak profiles – could not completely model their spectra. More recently, Long *et al.*[11] measured the $R(16)$ line from a tetrad CO_2 band [(30012) ← (00001)] near 1.6 μm and observed that both collisional narrowing and speed-dependent effects are necessary to describe the lineshape and reduce the fit residuals to the measurement noise level. This necessity for simultaneous collisional narrowing and speed-dependent effects was first demonstrated by Duggan *et al.*[14] for CO transitions. Similar observations were subsequently made for many other systems, including HF + Ar,[15] H_2 + Ar,[16] H_2O + Xe,[17] C_2H_2 + Xe,[18] H_2O + N_2,[19] and more recently O_2 + O_2.[20] This suggests a possible limitation in the analysis by Casa *et al.*[10] We extend this analysis to the 2.06 μm CO_2 band region to reconcile these observations.

SPECTRUM ANALYSIS

The purpose of this experiment is to quantify the physical effects governing the lineshapes of CO_2 in the (20013) ← (00001) vibrational band centered at 2.06 μm. The simplest profile considered here is the Voigt profile, which is the convolution of Gaussian (Doppler-broadened) and Lorentzian (pressure-broadened) profiles. Moreover, the complex Voigt profile (I_{VP}) has been defined previously.[21,22] When collisions with a perturber gas occur, other non-Voigt phenomena can arise. The first effect is Dicke (collisional) narrowing, which arises from velocity-changing collisions that effectively reduce the Doppler broadening contribution.[23] Rautian and Sobelman[24] incorporated Dicke narrowing by treating velocity-changing collisions as a combination of soft and hard collisions. Furthermore, assuming limiting cases that

[a)]Authors to whom correspondence should be addressed. Electronic addresses: tbui@caltech.edu; david.long@nist.gov; agata@fizyka.umk.pl; and mo@caltech.edu.

collisions are either soft or hard gives rise to the Galatry[25] (GP) and Nelkin–Ghatak[26] (NGP) profiles, respectively. The soft-collision model treats absorber motion as a diffusional process, whereas the hard collision model assumes a complete loss of velocity memory of the absorber after collisions. Although this assumption from the latter is non-physical, it results in the following convenient analytic form of the NGP in terms of the VP given by[24,26]

$$I_{\mathrm{NGP}}(u) = \frac{I_{\mathrm{VP}}{}^{*}(u)}{1 - \pi z I_{\mathrm{VP}}{}^{*}(u)}, \quad (1)$$

where $u = (\omega - \omega_0)/\omega_D$ is the reduced frequency, $z = \nu_{opt}/\omega_D$ is the reduced effective frequency of the velocity-changing collisions, ν_{opt}, and $I_{VP}{}^{*}$ is I_{VP} with the Lorentzian frequency halfwidth Γ (half width at half maximum – HWHM) expressed by a reduced variable $g = \Gamma/\omega_D$ replaced by $g + z$, following the notation from Ref. 23. ω_D is related to the Doppler frequency halfwidth, Γ_D (HWHM), by the equation $\Gamma_D = \omega_D\sqrt{ln2}$. In both the GP and NGP profiles, the relevant variable for fitting is the collisional narrowing parameter, β, which is a function of pressure, p, in terms of the collisional narrowing frequency ν_{opt}: $\beta(p) = \nu_{opt}/p$. It is important to note that both the GP and NGP profiles assume uncorrelated collisional perturbations (i.e., the collisions affect either molecular dephasing or velocity changes, but not both simultaneously).[27,28]

In addition to collisional narrowing (which causes symmetric changes in the lineshape if correlations between dephasing and velocity-changing collisions are neglected), collision time asymmetry[29–31] (which occurs when collisions are not treated as instantaneous) and line mixing[32,33] can introduce dispersion asymmetry in the lineshape center and near wings.[34] Finally, one must also consider the influence of speed-dependence of collisional broadening and line shifting on the resulting lineshape.[35–37] This effect generally causes a narrowing of the pressure-broadened line profile in addition to line asymmetry caused by speed dependence of line shifting. When such speed-dependent effects are considered, either the speed-dependent Voigt[35] (SDVP, Eq. (2)), speed-dependent Galatry (SDGP),[38] or speed-dependent Nelkin-Ghatak[39] (SDNGP, Eq. (3)) profiles are commonly used. Importantly, the SDGP and SDNGP include collisional narrowing, whereas the SDVP does not. The SDVP and SDNGP are given by[40]

$$I_{\mathrm{SDVP}}(u) = \frac{2}{\pi^{3/2}} \int_{-\infty}^{\infty} dx e^{-x^2} x \left(\arctan\left[\frac{u - dB_S(x) + x}{gB_W(x)}\right] + \frac{i}{2}\ln\left\{1 + \left[\frac{u - dB_S(x) + x}{gB_W(x)}\right]^2\right\}\right), \quad (2)$$

and

$$I_{\mathrm{SDNGP}}(u) = \frac{I_{\mathrm{SDVP}}{}^{*}(u)}{1 - \pi z I_{\mathrm{SDVP}}{}^{*}(u)}. \quad (3)$$

In Eq. (2) $d = \Delta/\omega_D$ is the reduced collisional shift, Δ, and $B_S(x)$ and $B_W(x)$ are dimensionless functions for the reduced speed-dependent shifts and widths, respectively, and x is the reduced absorber speed (the ratio of the actual to the most probable speed). It was previously shown that if the interaction potential for the absorber-perturber pair is given by an inverse power relationship, C/r^q, the expressions for $B_S(x)$ and $B_W(x)$ can be written in terms of confluent hypergeometric functions.[35,36] A common quadratic approximation is used to simplify these reduced speed-dependent functions with respect to the speed-dependent width and shift parameters (a_W and a_S, respectively, which are also used as fitted parameters),[41,42] shown more explicitly as

$$\begin{aligned} B_W(x) &= \frac{\Gamma(v_A)}{\Gamma} = 1 + a_W\left(x^2 - \frac{3}{2}\right) \\ B_S(x) &= \frac{\Delta(v_A)}{\Delta} = 1 + a_S\left(x^2 - \frac{3}{2}\right) \end{aligned}. \quad (4)$$

Here, $\Gamma(v_A)$ and $\Delta(v_A)$ are the collisional widths and shifts as a function of absorber velocity, v_A. One may easily show that for systems containing more than one perturber, total reduced speed-dependent functions $B_W(x)$ and $B_S(x)$ are also given in the quadratic form. In this case, the a_W and a_S parameters for a gas mixture are weighted averages of the corresponding parameters for individual perturbing gases.[43]

Finally, when correlations between velocity-changing and dephasing collisions[24] are important, a partially correlated speed-dependent profile (pCSDNGP), introduced by Pine[15] can be used. This profile, $I_{pCSDNGP}(u)$, is expressed in the same way as Eq. (3),[44] but differs in the definition of the complex narrowing parameter, ν_{opt}.[24,27,45–47] In the $I_{pCSDNGP}(u)$, ν_{opt} is given by $\nu_{opt} = \nu_{diff} - \eta_\Gamma \Gamma - i\eta_\Delta \Delta = \mathrm{Re}(\nu_{opt}) + i\mathrm{Im}(\nu_{opt})$, where the velocity dependence of Γ and Δ parameters was neglected.[27] ν_{diff} is the frequency of velocity-changing collisions calculated from the mass diffusion coefficient. The real and imaginary parts of ν_{opt} are designated as $\mathrm{Re}(\nu_{opt})$ and $\mathrm{Im}(\nu_{opt})$, respectively. The correlation parameters, η_Γ and η_Δ, correspond to collisional broadening and shifting, respectively. In the case of no correlation, η_Γ and η_Δ parameters are equal to zero and $\nu_{opt} = \nu_{diff}$.

For the CO_2-air system probed in this experiment, the ratios of the perturber (O_2 and N_2) to absorber (CO_2) mass are $m_{O2}/m_{CO2} = 0.73$ and $m_{N2}/m_{CO2} = 0.64$; therefore, the absorber is only slightly heavier. Using the diffusion coefficient of CO_2 in air $D = 0.159$ cm^2 s^{-1} ($p = 101.325$ kPa, $T = 296$ K),[48] the mean-free-path of CO_2 can be calculated as $l_{mfp} = 3D/\bar{v}$, where $\bar{v}$ is the relative mean velocity of the perturber-absorber pair. For $T = 296$ K, $p = 26.7$ kPa, the mean-free-path of CO_2 is calculated to be $l_{mfp} = 0.341$ μm, which is much smaller than the optical wavelength of 2.06 μm. This suggests that collisional narrowing must also be considered. To facilitate studies of isolated lineshapes, measurements were made at sufficiently low pressures (i.e., 7 kPa–28 kPa) such that line mixing effects could be neglected. Nevertheless, all other stated effects are accessible in this pressure range.

EXPERIMENT

Measurements were performed using a 2.06 μm frequency-stabilized cavity ring-down spectrometer (FS-CRDS) located at the California Institute of Technology (see Fig. 1(a)). The spectrometer is based on the design of Hodges

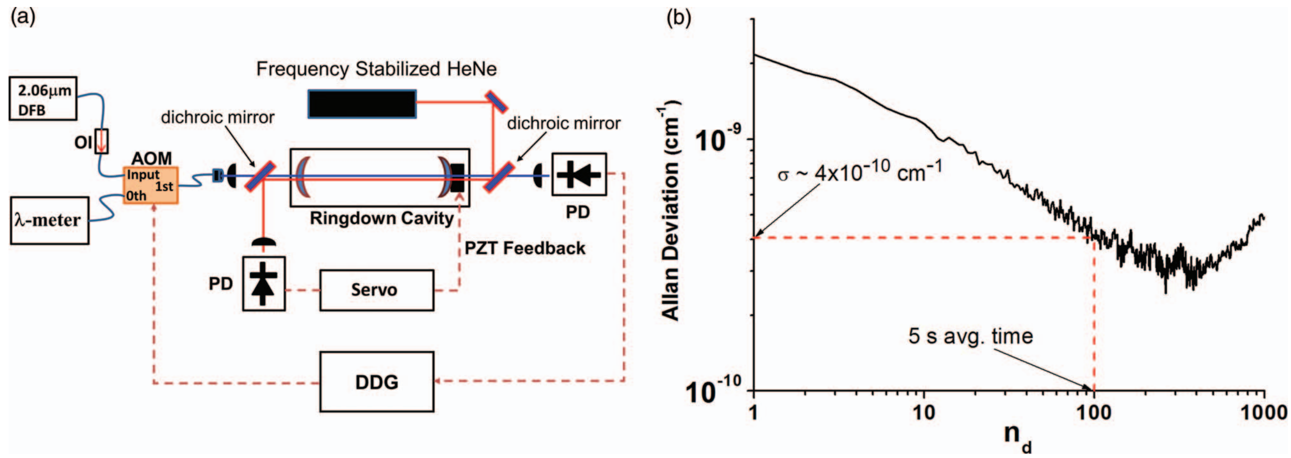

FIG. 1. (a) Schematic of the 2.06 μm frequency-stabilized cavity ring-down spectrometer. OI = optical isolator, PD = photodiode, AOM = acousto-optic modulator, DDG = digital delay generator. 2.06 μm light is injected into a fiber-coupled AOM and subsequently free-space coupled into the ring-down cavity. Once the transmitted light intensity reaches a threshold, a DDG shuts off the light to initiate the ring-down. Light from a frequency-stabilized HeNe laser is counter-propagated through the cavity and is used to stabilize the cavity's length. (b) Allan deviation plot for the 2.06 μm FS-CRDS spectrometer. The *x*-axis displays the number of ring-down traces (acquired at an acquisition rate of ≈20 Hz), n_d, at a given frequency. The *y*-axis gives the Allan deviation corresponding to the baseline losses. For typical experimental conditions, 100 ring-down traces were acquired, corresponding to a minimum detectable absorption of $\approx 4 \times 10^{-10}$ cm^{-1}.

et al.[49–51] Briefly, the ring-down cavity was actively locked to a temperature-stabilized HeNe laser with an optical frequency stability of 100 kHz (8 h). The probe laser was a distributed-feedback diode laser (≈3 mW power) centered at 2.055 μm. The fiber-pigtailed output was sent through a fiber-optic isolator and then into a fiber-coupled acousto-optic modulator (AOM). The 1st order output from the AOM was free-space coupled via a single focusing lens (f = 500 mm) into the ring-down cavity. The 0th-order output was free-space coupled into a wavelength meter with a standard uncertainty of 30 MHz. Light exiting the ring-down cavity was focused onto an adjustable-gain, extended InGaAs detector with a maximum bandwidth of 1 MHz.

For these experiments, the ring-down mirrors had dichroic coatings: reflectivity R ≈ 99.99% at 2.06 μm, corresponding to a vacuum finesse of ≈31 000, and R ≈ 95% at 0.633 μm. As many as 100 ring-down traces of $\tau \approx 26$ μs were acquired using a fast fitting algorithm[52] at a rate of 20 Hz–30 Hz and averaged at each wavelength, corresponding to a minimum detectable absorption coefficient of $\approx 4 \times 10^{-10}$ cm^{-1} (see Fig. 1(b)). The cavity's free spectral range (FSR) was measured by the method of Lisak and Hodges[53] to be 203.890(82) MHz. This pressure-corrected value sets the frequency spacing between the spectrum data points.

The gas sample was composed of CO_2 in air with a mixing ratio of ≈90 μmol mol^{-1} at pressures of 7 kPa–27 kPa as measured by a capacitance manometer (full-scale range of 133.32(13) kPa). The air content contained 20.9% oxygen with the remainder being nitrogen. The cavity temperature was monitored by a 2.252 kΩ thermistor and displayed short-term (i.e., the time required to record a single spectral line) fluctuations less than 100 mK. All measurements were performed within the temperature range of 295.4 K–296.1 K. Since this value is close to the HITRAN reference temperature of T_{ref} = 296 K,[54] the uncertainties in the temperature corrections to the air-broadening coefficients were negligible compared to the fit uncertainties.

RESULTS AND DISCUSSION

In this section we present the results from a thorough lineshape analysis for two selected air-broadened lines from the (20013) ← (00001) CO_2 band centered near 2.06 μm, specifically the R(24) line at 4871.791 cm^{-1} and the R(30) line at 4875.749 cm^{-1}. The CO_2-air mixture pressure range was 48.1–210 Torr (6.5–28 kPa) for the R(24) line and 48.1–180.3 Torr (6.5–24 kPa) for the R(30) line. The R(30) line was chosen because it is a potential target for the ASCENDS[3] mission, while the R(24) line is more ideal for lineshape analysis because of its isolation from isotopic interferences. The two selected lines are shown in Fig. 2. Note that for the R(30) line at 4875.749 cm^{-1}, a $^{13}CO_2$ isotopologue in the right wing presents the main interference with a line intensity that is 6.2% of the main isotopologue transitions.[54]

Beyond the normally used Voigt profile, we have incorporated into our lineshape analysis more advanced profiles that take into account line narrowing effects as well as lineshape asymmetries. For each of the fits, the Doppler widths were calculated from the known temperature around 296 K and were held fixed. In addition, the collisional shifts were set to the HITRAN2012[54] values found in Table I. Residuals from the single-spectrum fit analysis for the different lineshape models are presented in Fig. 2 for four intermediate pressures. The VP gives the worst fit with the residuals exhibiting a large systematic feature indicative of line narrowing. Upon including Dicke narrowing (i.e., the GP and NGP fits), the large residuals observed with the VP disappear. Similar results were obtained for the SDVP fit which uses a different mechanism of line narrowing, namely, the speed dependence of collisional broadening. For a better comparison of the fit results provided by the different lineshape models, we introduced a quality of fit factor for multi-spectrum fits,[20] QF_{multi}, defined as the ratio of the peak absorption signal for the spectrum having the highest absorption, $\mathrm{Max}_j\{\alpha_{\max,j} - \alpha_{\min,j}\}$, to the standard deviation $\tilde{S}_{R_{\mathrm{multi}}}$ of the fit residuals

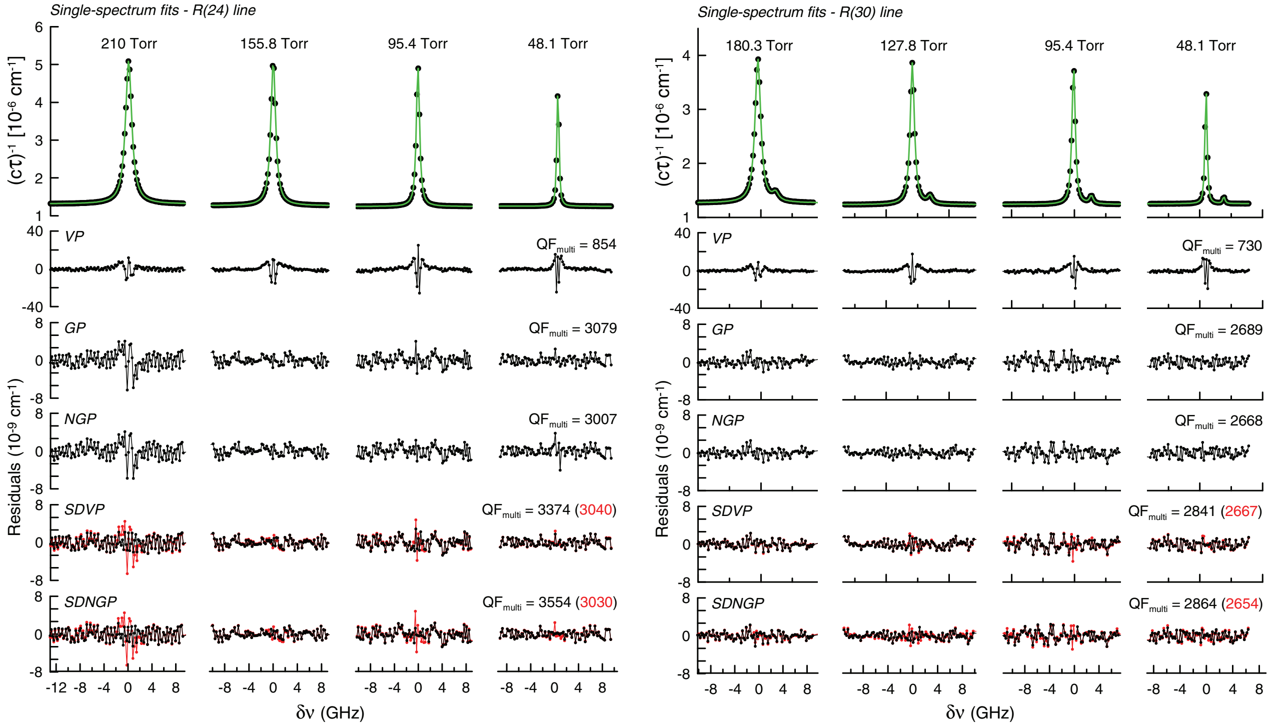

FIG. 2. Four representative single spectrum fits for the $R(24)$ and $R(30)$ transitions using a variety of line profiles. The upper panel shows the measurement and the corresponding single-spectrum fit using the SDNGP. The bottom five panels show the fit residuals for the VP, GP, NGP, SDVP, and SDNGP, respectively. The black and red residuals presented for the SDVP and SDNGP fits are with ($a_S \neq 0$) and without ($a_S = 0$) the speed dependence of collisional shifts, respectively. $\delta\nu$ on the x-axis corresponds to the frequency detuning from line centers in GHz.

calculated from all of the spectra included in the multi-spectrum fit:

$$QF_{\text{multi}} = \frac{\text{Max}_j\{\alpha_{\max,j} - \alpha_{\min,j}\}}{\tilde{S}_{R_{\text{multi}}}}. \tag{5}$$

In the above expression, $\alpha_{\max,j}$ is the maximum absorption coefficient and $\alpha_{\min,j}$ is the baseline level of the absorption spectrum for the jth spectrum. $\tilde{S}_{R_{\text{multi}}}$ is the standard deviation of the fit residuals calculated from the formula

$$\tilde{S}_{R_{\text{multi}}} = \sqrt{\frac{1}{\sum_{j=1}^{N} M_j - k}\sum_{j=1}^{N}\sum_{i=1}^{M_j}[\alpha_{\exp}(\nu_{ji}) - \alpha_{\text{fit}}(\nu_{ji})]^2}, \tag{6}$$

where N is the number of spectra taken included in the multi-spectrum fit, M_j is the number of points in the jth spectrum ($j = 1, \ldots, N$) and $\sum_{j=1}^{N} M_j - k$ is the total number of degrees of freedom with k lineshape parameters fitted in the multi-spectrum fit procedure. The terms $\alpha_{\exp}(\nu_{ji})$ and $\alpha_{\text{fit}}(\nu_{ji})$ are experimental and fitted absorption coefficients, respectively, for the ith measurement point in the jth spectrum.

Based upon the residuals from single-spectrum fits, we observed that Dicke narrowing and speed-dependent effects describe the narrowing mechanism of the CO_2 lineshapes equally well. In addition, under conditions of low and intermediate ratios of the collisional width, Γ, to the Doppler width, Γ_D, the lineshape affected by the speed dependence of collisional broadening can often be well modeled by the Dicke narrowed profile.[41,55] Unfortunately, this treatment leads to a nonlinear pressure dependence of the narrowing parameter Re(ν_{opt})[14,56,57] in this intermediate case (i.e., $1 < \Gamma/\Gamma_D < 5$). This nonphysical result can be seen in the $R(24)$ NGP fit shown in Fig. 3(a).

On the other hand, a reduction of the observed a_W parameter with pressure in the SDVP fits, presented in Fig. 3(b), suggests that Dicke narrowing also contributes to the shape of both the $R(24)$ and $R(30)$ lines. Consequently, the data were also analyzed with the SDNGP, which includes both of these narrowing effects. Residuals from this single-spectrum

TABLE I. Lineshape parameters for the $R(24)$ and $R(30)$ lines obtained from the pCSDNGP multi-spectrum fit analysis at $T_{\text{avg}} = 295.72$ K. Line positions, ν_0, and collisional shift coefficients, Δ/p, used in the data analysis are taken from measured values by Toth et al.,[69,70] which are found in the HITRAN database. The stated uncertainties of the lineshape parameters arise from the uncertainty in the fit. The correlation parameters, η_Γ and η_Δ, obtained from the pCSDNGP profile are stated in the text.

Line	ν_0 (cm^{-1}) HITRAN	Δ/p (cm^{-1}/atm) HITRAN	$2\Gamma/p$ (cm^{-1}/atm)	Re(ν_{opt})/p (cm^{-1}/atm)	Im(ν_{opt})/p (cm^{-1}/atm)	a_W	a_S
$R(24)$	4871.791 674	−0.005 683	0.074 682(33)	0.001 34(60)	0.002 90(40)	0.0799(21)	0.2080(170)
$R(30)$	4875.748 732	−0.005 859	0.0731 29(33)	0.002 48(18)	− 0.000 10(30)	0.0786(13)	0.0750(140)

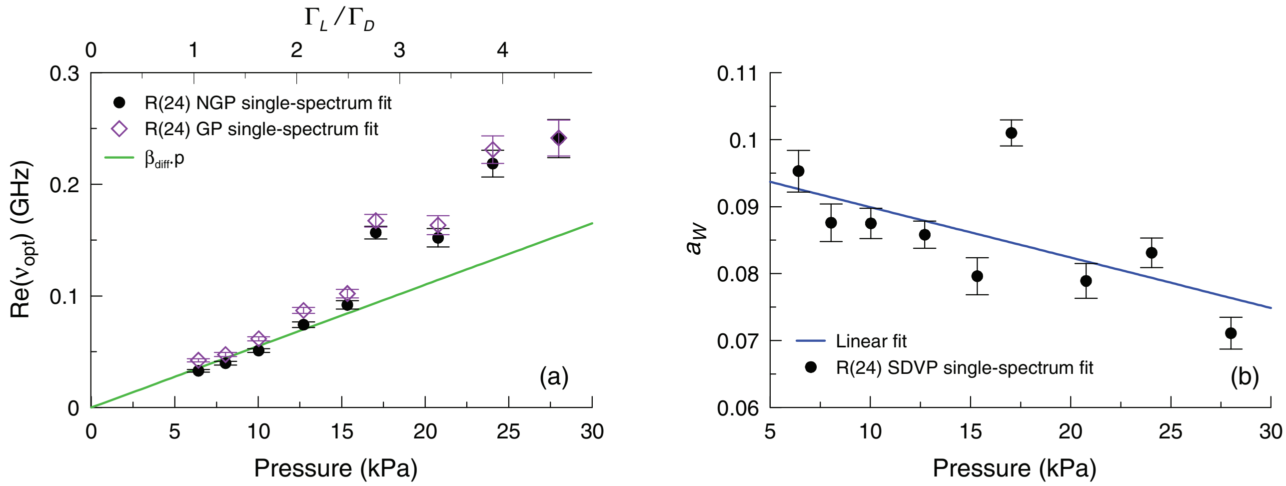

FIG. 3. Pressure dependence of the frequency of optical collisions, Re(ν_{opt}), and speed-dependence parameter, a_W, parameter obtained for the $R(24)$ line from the NGP, GP, and SDVP single-spectrum fits, respectively. The green line is the frequency of optical collisions, ν_{diff}, calculated from the mass diffusion coefficient. The blue line is a linear fit to data. Note that the given error bars arise only from the uncertainty in the fit, and that the additional scatter in the data is from instrumental effects.

fit analysis with the SDNGP are presented in Fig. 2, and are similar to those obtained when using the GP, NGP, and SDVP. Moreover, we noticed that the incorporation of the speed dependence of collisional shifting (which describes lineshape asymmetry) into the fits with the SDNGP and SDVP led to a further improvement of the residuals.

It should be noted, however, that flat residuals obtained from these single-spectrum fits do not guarantee proper interpretation of the lineshape effects in the measured spectra. Systematic instrumental errors may affect the shape of the investigated lines and can be well masked by nonlinear pressure dependencies of the fitted lineshape parameters as well as lineshape asymmetries. Also in the case of relatively complex profiles like the SDNGP, numerical correlations between the different lineshape parameters can become important and lead to a large scatter in the obtained results. It will be shown later that a multi-spectrum fit analysis[58] helps to overcome these problems.[59,60]

We note that the choice of line profile not only affects the fit residuals but also has a strong effect upon the resulting fitted parameters. In Fig. 4 deviations in the collisional widths and areas obtained for the $R(24)$ and $R(30)$ lines from the single-spectrum fit analysis with the VP, GP, NGP, and SDVP relative to the SDNGP are shown. The VP fit differs by as much as 5% and 1.2% from the SDNGP for the collisional width and area, respectively. The maximum deviations of the GP, NGP, and SDVP from the SDNGP for the collisional widths and areas are of the order of 0.7% and 0.2%, respectively. Moreover, the VP fit results do not converge with the other profiles even at high pressures, which indicates that the VP is not suitable for high accuracy measurements. This finding is consistent with previous observations by Long *et al.*[11] for CO_2 lines near 1.6 μm as well as for other systems.[16,19,57,59,61,62]

As shown in Fig. 2, the single-spectrum fit analysis with the SDNGP can reproduce the investigated spectra down to the instrument noise level. However, the large scatter in the fitted values for the Re(ν_{opt}) and a_W parameters presented in Fig. 6 indicate that they may be correlated. This competition of speed dependence of collisional broadening with collisional narrowing, particularly at low pressures, has been reported in a number of previous studies.[11,17–19,41,55]

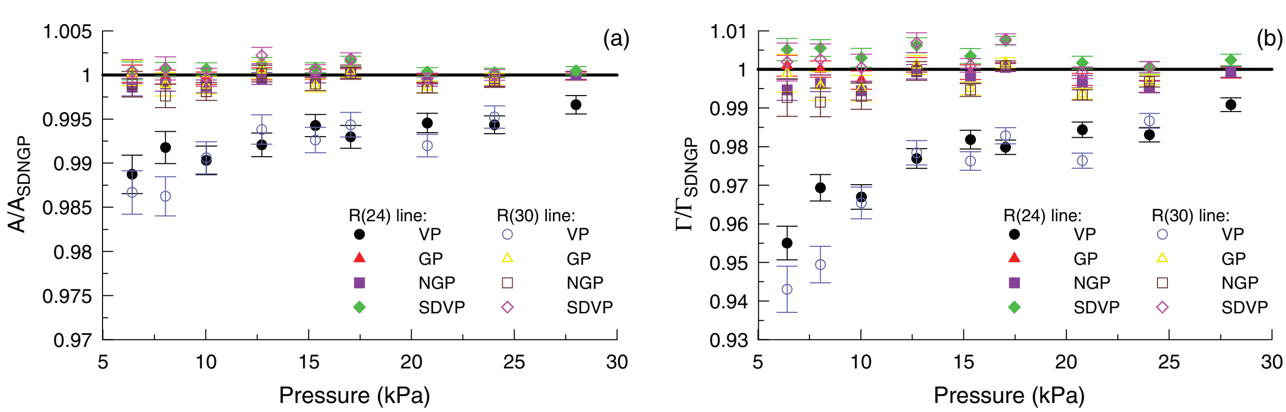

FIG. 4. Pressure-dependent integrated area and air-broadened collisional width ratios of the VP, GP, NGP, and SDVP to the SDNGP, denoted as A/A_{SDNGP} and Γ/Γ_{SDNGP}, respectively. Both the $R(24)$ and $R(30)$ lines are shown. The error bars arise from the uncertainty in the fit.

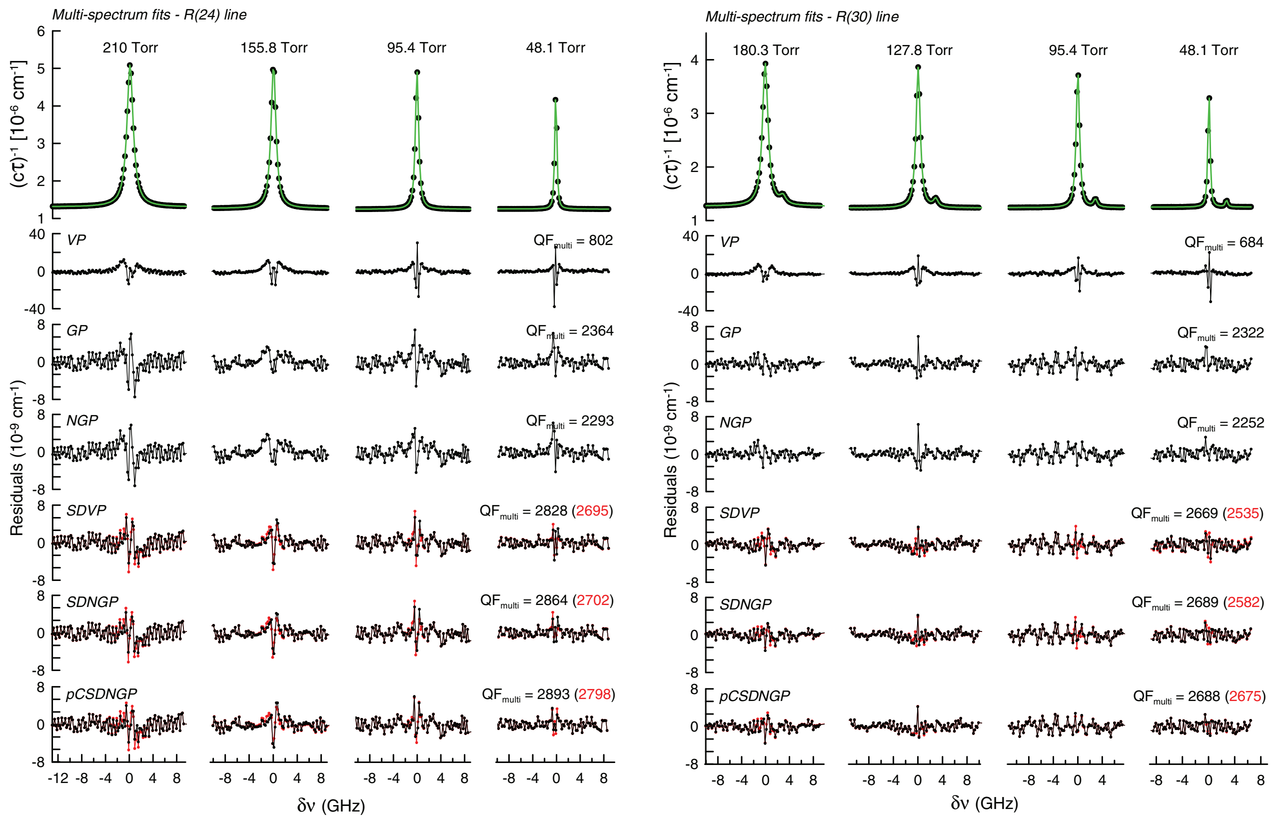

FIG. 5. Four representative multi-spectrum fits for the $R(24)$ and $R(30)$ transitions using a variety of line profiles. The upper panel shows the measurement and the corresponding fit using the pCSDNGP. The bottom six panels show the fit residuals for the VP, GP, NGP, SDVP, SDNGP, and pCSDNGP, respectively. The black and red residuals presented for SDVP, SDNGP, and pCSDNGP fits are with ($a_S \neq 0$) and without ($a_S = 0$) the speed dependence of collisional shifts, respectively. $\delta\nu$ on the x-axis corresponds to the frequency detuning from line centers in GHz.

A solution to remove correlation between the Re(ν_{opt}) and a_W parameters is to incorporate a multi-spectrum fit procedure[58] into the lineshape analysis.[44,59,60,63,64] Therefore, we performed simultaneous fits to the nine spectra from 6.5–28 kPa for the $R(24)$ line and eight spectra from 6.5–24 kPa for the $R(30)$ line with a few necessary constraints. First, the collisional widths and frequencies of optical collisions were constrained to be linear with pressure according to the relations $\Gamma(p) = \gamma p$ and $\nu_{opt}(p) = \beta p$, where γ and β are the collisional broadening and collisional narrowing coefficients, respectively, fitted in the multi-spectrum analysis. Moreover, in the case of the speed-dependent profiles, singular values for the a_W and a_S parameters were fitted for all pressures to assure their pressure independences. Due to the small fluctuations of CO_2 concentration in the CO_2-air mixture, the spectral areas were fitted individually for each pressure.

Figure 5 shows the representative residuals from the multi-spectrum fit analyses for the $R(24)$ and $R(30)$ lines. Similar to the single-spectrum fit analysis, the VP gave the worst results. However, contrary to the single-spectrum analysis, the fits residuals for the profiles which describe different mechanisms of line narrowing are now distinguishable. Comparing the QF_{multi} for the GP and NGP, it appears that the soft collision model better describes the line narrowing effect for both investigated lines. On the other hand, the large improvements in the QF_{multi} for the SDVP without the speed dependence of collisional shifting ($a_S = 0$) by as much as 12% and 8% for the $R(24)$ and $R(30)$ lines, respectively, compared to the GP suggest the dominant contribution of speed dependence of collisional broadening into the total narrowing of these lines. It was also observed that the incorporation of Dicke narrowing improves the QF_{multi} compared to the SDVP (with $a_S = 0$). In addition, the incorporation of the speed dependence of collisional shifting in the SDVP and SDNGP analysis improved the residuals and led to a further increase of the QF_{multi}. However, the contribution of speed-dependent asymmetry into the shape of the $R(24)$ and $R(30)$ lines appears to be weaker for the multi-spectrum fits than for the single-spectrum ones.

A comparison of the differences between the QF_{multi} improvements obtained from SDNGP fits with ($a_S \neq 0$) and without ($a_S = 0$) speed-dependent asymmetry in the case of the single- and multi-spectrum fit analysis gave the following results: 15% and 7% for the $R(24)$ line and 7% and 4% for the $R(30)$ line, respectively. These differences suggest that the observed lineshape asymmetry is caused partially by instrumental effects and is integrally simulated by the speed-dependent asymmetry in the single-spectrum fit analysis. Note also that the asymmetry differences between single- and multi-spectrum fits are larger for the $R(24)$ line, which are attributed to a larger contribution of instrumental errors to the total line shape.

As previously shown by Lisak *et al.*,[63] the utility of multi-spectrum fitting in advanced lineshape analysis can be demonstrated from a simple test of the fitted parameters. From Fig. 6, the large pressure variations of the Re(ν_{opt}) and

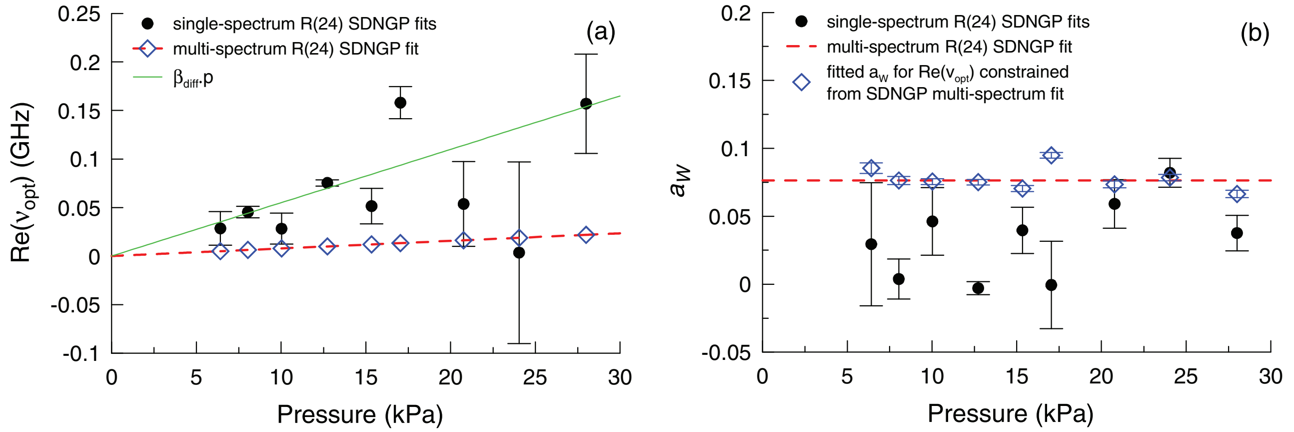

FIG. 6. A test of the multi-spectrum fit parameters for Re(ν_{opt}) and a_W. The black points represent the parameter values obtained from the SDNGP single-spectrum fit analysis. Numerical correlations between Re(ν_{opt}) and a_W parameters are evident from the large scatter. The red dashed lines are the Re(ν_{opt}) and a_W values yielded by the SDNGP multi-spectrum fit. The blue diamonds in graph (a) correspond to Re(ν_{opt}) from the SDNGP multi-spectrum fit. The blue diamonds in graph (b) correspond to a_W parameters fitted individually for each pressure in the SDNGP single-spectrum fit analysis when Re(ν_{opt}) is constrained to the value from the SDNGP multi-spectrum fit. The green solid line is the frequency of optical collisions ν_{diff} calculated from the mass diffusion coefficient.[48]

a_W parameters for the R(24) line are suggestive of strong numerical correlations between them. The black points correspond to the parameters obtained from the SDNGP single-spectrum fits with Re(ν_{opt}) and a_W both fitted. The straight dashed lines are the Re(ν_{opt}) and a_W values obtained from the SDNGP multi-spectrum fit. The blue diamonds in Fig. 6(b) correspond to single-spectrum fits of the SDNGP in which the Re(ν_{opt}) was constrained to the value from the multi-spectrum fit and a_W was fitted individually for each pressure. Consequently, the fitted a_W is expected and observed to be nearly pressure-independent. Moreover, the large scatter in the fitted values of a_W and their uncertainties are significantly reduced. Therefore, the additional constraints provided by the multi-spectrum fitting procedure was necessary to properly treat the correlations between the Re(ν_{opt}) and a_W parameters.

The green solid lines plotted in Figs. 3(a) and 6(a) correspond to the frequency of velocity-changing collisions calculated from the mass diffusion coefficient[48] (ν_{diff} = 5.5 kHz/Pa). By comparing the ν_{diff} and Re(ν_{opt}) values, one may estimate the contribution of correlation between velocity- and phase-changing collisions (v-p correlations) into the lineshapes of the investigated CO_2 lines. In Fig. 3(a), the Re(ν_{opt}) values obtained from NGP single-spectrum fits agree with ν_{diff} for pressures up to 12 kPa. This incidental agreement can suggest that there is no need for inclusion of v-p correlations or speed dependence of collisional broadening for the R(24) line. However, such conclusion can be incorrect as first shown by Duggan *et al.*[61] for CO lines. We have already shown that the NGP is inadequate for modeling the data, and that the speed dependence of collisional broadening has a much greater contribution to the total narrowing of lineshapes than the Dicke narrowing effect. Moreover, the retrieved value of the Re(ν_{opt}) from the SDNGP multi-spectrum fit, presented in Fig. 6(a) as the red dashed line, is almost one order of magnitude smaller than ν_{diff}. This is indicative of v-p correlations for the R(24) line. Similar conclusions were drawn for the R(30) line.

Correlations between phase- and velocity-changing collisions (v-p correlations) are another source of lineshape asymmetry and cannot be ignored when asymmetry has been observed. To properly account for v-p correlations, we performed the multi-spectrum fit analysis with the partially correlated SDNGP (pCSDNGP) for both investigated lines. The residuals and QF_{multi} values from the pCSDNGP fits are presented in Fig. 6 and are observed to be similar to those obtained from the SDNGP analysis. It should be noted that both mechanisms of lineshape asymmetry, namely, the speed dependence of collisional shifting and v-p correlations, were considered in the presented fits. A comparison of the QF_{multi} factors for the pCSDNGP with ($a_S \neq 0$) and without ($a_S = 0$) speed-dependent asymmetry shows that the speed-dependent asymmetry can be well simulated by the v-p correlation asymmetry. To quantify the contribution of the v-p correlations into the total narrowing and asymmetry, we calculated the correlation parameters, η_Γ and η_Δ, based on the ν_{diff} value and pCSDNGP multi-spectrum parameters of Re(ν_{opt}), Im(ν_{opt}), Γ, and Δ. The results are $\eta_\Gamma = (0.231 \pm 0.008)$, $\eta_\Delta = (0.51 \pm 0.12)$ for the R(24) line and $\eta_\Gamma = (0.2202 \pm 0.0024)$, $\eta_\Delta = (-0.024 \pm 0.051)$ for the R(30) line. The small relative uncertainties of the η_Γ parameters of about 3% and 1% for the R(24) and R(30) lines, respectively, confirm the occurrence of v-p correlations in the shape of investigated CO_2 lines. Moreover, a small value for η_Δ obtained for the R(30) line suggests that there is minimal v-p correlation asymmetry for this line. This is also confirmed by a relatively small difference between QF_{multi} obtained from the pCSDNGP analysis with ($a_S \neq 0$) and without ($a_S = 0$) speed-dependent asymmetry. On the other hand, the η_Δ value for the R(24) line is surprisingly high. However, the slightly worse residuals obtained for the R(24) line indicate that additional lineshape asymmetry may be introduced by instrumental errors. It should be noted that the collisional shift, Δ, is a much smaller effect than collisional broadening Γ; therefore, a quantitative analysis of Im(ν_{opt}) and a_S is more challenging experimentally than analysis of Re(ν_{opt}) and a_W.

A test of the multi-spectrum fit parameters of Im(ν_{opt}) and a_S describing v-p correlations and speed-dependent asymmetries, respectively, is demonstrated in Fig. 7. The

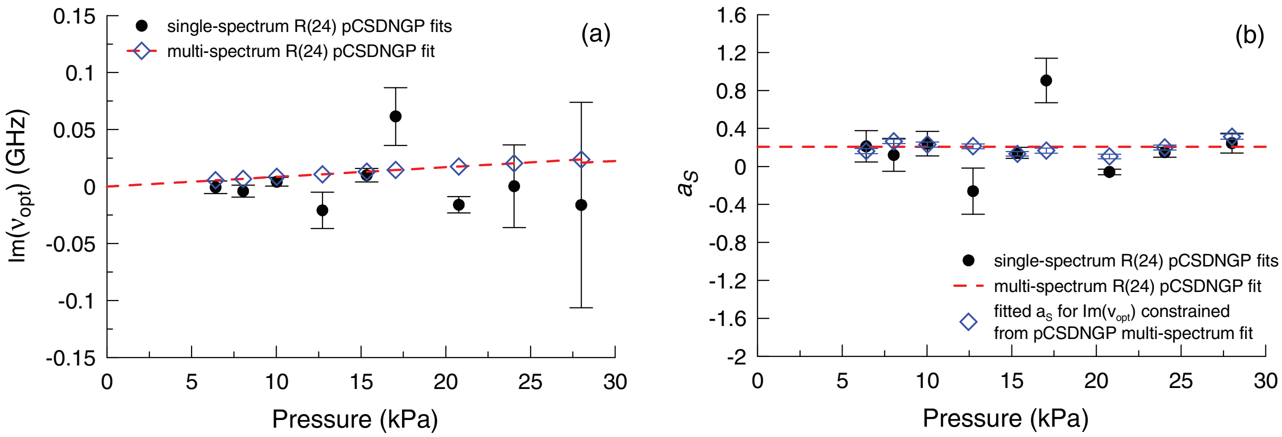

FIG. 7. A test of the multi-spectrum fit parameters $\mathrm{Im}(\nu_{\mathrm{opt}})$ and a_{S}. The black points are the parameters obtained from the pCSDNGP single-spectrum fit analysis. Numerical correlations between the $\mathrm{Im}(\nu_{\mathrm{opt}})$ and a_{S} parameters in the single-spectrum fits are evident from the large scatter. The red dashed lines are the $\mathrm{Im}(\nu_{\mathrm{opt}})$ and a_{S} values yielded by the pCSDNGP multi-spectrum fit. The blue diamonds in graph (a) correspond to $\mathrm{Im}(\nu_{\mathrm{opt}})$ from the pCSDNGP multi-spectrum fit. The blue diamonds in graph (b) correspond to the a_{S} parameters fitted individually for each pressure in the pCSDNGP single-spectrum fit analysis where $\mathrm{Im}(\nu_{\mathrm{opt}})$ is constrained to the value from the pCSDNGP multi-spectrum fit.

black points show the fitted $\mathrm{Im}(\nu_{\mathrm{opt}})$ and a_{S} values obtained from the pCSDNGP single-spectrum fits. The large scatter suggests that they are correlated. The red dashed lines are the $\mathrm{Im}(\nu_{\mathrm{opt}})$ and a_{S} values obtained from the pCSDNGP multi-spectrum fit. The blue diamonds in Fig. 7(b) correspond to single-spectrum fits of the pCSDNGP in which the $\mathrm{Im}(\nu_{\mathrm{opt}})$ was constrained to the value from the pCSDNGP multi-spectrum fit, and a_{S} was fitted for each pressure. In addition, we constrained the pressure dependence of $\mathrm{Re}(\nu_{\mathrm{opt}})$ and the pressure independence of a_{W}, and we fixed their values to those obtained from the pCSDNGP multi-spectrum fit. As observed before, the fitted a_{S} are nearly independent on pressure and the scatter in the fitted values of a_{S} is greatly reduced when $\mathrm{Im}(\nu_{\mathrm{opt}})$ is constrained to the value from the multi-spectrum fit. The recommended parameters describing the shape of the $R(24)$ and $R(30)$ lines, obtained from the pCSDNGP multi-spectrum fits, are assembled in Table I.

Comparisons of the integrated line areas per unit pressure and the collisional air-broadening coefficients retrieved from the multi-spectrum fit analysis with the use of different lineshape models in relation to the pCSDNGP are presented in Fig. 8. The VP differs from the pCSDNGP by 0.6% and 2% for the line area and collisional broadening coefficient, respectively. The GP, NGP, and SDVP differ from the pCSDNGP by less than 0.1% for the line area. However, for the Γ values, the GP and NGP results differ by more than 0.6% from the pCSDNGP, whereas for the SDVP the difference is only about 0.1%. The areas and collisional broadening coefficients obtained from the SDNGP are very close to those retrieved from the pCSDNGP. It should be noted that collisional air-broadening coefficients given in the HITRAN2012 database are systematically lower by almost 6% and 2% compared to values obtained from pCSDNGP and VP fits, respectively. Note that the error bars presented in Fig. 8 arise from the uncertainty in the fit. Moreover, the large error bars of $\Gamma/\Gamma_{\mathrm{pCSDNGP}}$ for the HITRAN2012 case correspond to a reported 2% relative uncertainty of the collisional air-broadening coefficient. Finally, observed fluctuations of the CO_2 concentration in the CO_2-air mixture measurements are responsible for the large uncertainty of area per unit pressure

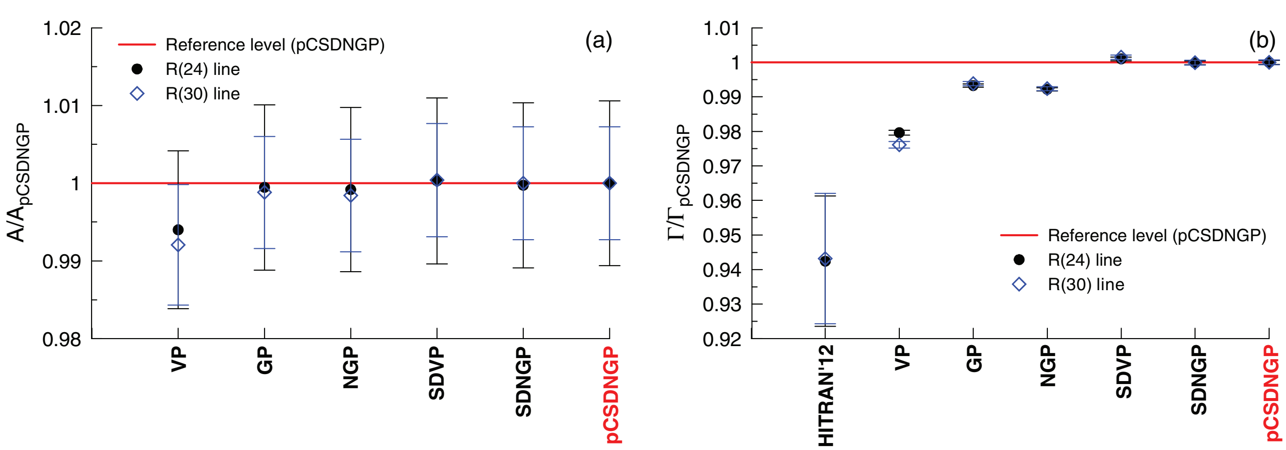

FIG. 8. A comparison of the fitted line areas per unit pressure (a) and collisional air-broadening coefficients (b) retrieved from the multi-spectrum fit analysis with the use of different lineshape models in relation to the pCSDNGP. Both the $R(24)$ and $R(30)$ lines are shown. In case of the collisional broadening coefficient, differences between the recommended pCSDNGP and HITRAN2012 values are also presented. The shown uncertainties are the fit uncertainties.

coefficient and also for the large error bars of $A/A_{pCSDNGP}$ for all of the investigated lineshape models.

CONCLUSIONS

A lineshape analysis of two air-broadened rovibrational CO_2 transitions near 2.06 μm was performed with spectra recorded with a frequency-stabilized cavity ring-down spectrometer. Two main line narrowing mechanisms – velocity-changing collisions and the speed dependence of collisional broadening – were identified in the total lineshape. To quantify the individual contribution from both narrowing effects and remove their correlation, the multi-spectrum fit technique was incorporated into the SDNGP lineshape analysis. In addition, a noticeably smaller value of the frequency of optical collisions retrieved from the SDNGP multi-spectrum fit compared to the value calculated from the mass diffusion coefficient revealed evidence of correlations between the phase- and velocity-changing collisions for both the $R(24)$ and $R(30)$ transitions. Moreover, small asymmetries in the lineshapes were also observed. However, this asymmetry can be equally well ascribed to either the speed dependence of collisional shifting or to the correlations between phase- and velocity-changing collisions. Consequently, we concluded that the partially correlated SDNGP (pCSDNGP)[15] profile is the most appropriate model considered here to reproduce the experimental lineshapes at a high quality level. Experimental tests of pCSDNGP have also recently been reported for O_2[44] and H_2O.[65] Furthermore, efficient algorithms for calculating the pCSDNGP line profile have been developed[28,66,67] and is strongly recommended for modeling lineshapes in the spectrally isolated regime.[68] We note that an alternative nomenclature in the literature for the same pCSDNGP profile used here is the partially correlated speed-dependent hard-collision profile.[65] In the case of quadratic speed-dependence, the following names were used as well: partially correlated quadratic-speed-dependent hard-collision profile (pCqSDHCP),[28,66–68] partially correlated quadratic-speed-dependent Nelkin-Ghatak profile,[43] and Hartmann-Tran profile (HTP).[68]

Experimental data were also fitted with the commonly used VP. However, we showed that it is not sufficient for modeling CO_2 transitions with the accuracy and precision demanded in remote sensing applications. We noticed 2% and 4% biases introduced by the VP in the retrieved air-broadening parameters compared to the values obtained from the recommended pCSDNGP and HITRAN2012 database. Moreover, it is interesting and remarkable that lineshape models incorporating only the Dicke narrowing effect (GP, NGP) provide systematically lower values of collisional air-broadening coefficients by about 0.6% compared to pCSDNGP. Finally, we acknowledge the necessity of more comprehensive lineshape models that incorporate collisional line-mixing at higher pressures for utility of the broader remote sensing community.

ACKNOWLEDGMENTS

This work was supported by the Orbiting Carbon Observatory-2 (OCO-2) project at the Jet Propulsion Laboratory under contract with the National Aeronautics and Space Administration (NASA) through the NASA grant NAS7-03001. T.Q.B. was supported by a NASA Earth and Space Sciences Fellowship and the NASA Mars Fundamental Research Grant NNX12AI01G. D.W.H. was supported by the Jack and Edith Roberts Summer Undergraduate Research Fellowship. Support for D.A.L. and V.T.S. was provided by the NIST Greenhouse Gas Measurements and Climate Research Program. A.C., D.L., and R.C. were partially supported by the Foundation for Polish Science TEAM Project co-financed by the EU European Regional Development Fund, the National Science Centre, Project Nos. DEC-2011/01/B/ST2/00491 and UMO-2013/11/D/ST2/02663, and is part of the program of the national laboratory FAMO in Toruń, Poland. A.C. was further supported by the Foundation for Polish Science START Project.

[1]C. E. Miller, D. Crisp, P. L. DeCola, S. C. Olsen, J. T. Randerson, A. M. Michalak, A. Alkhaled, P. Rayner, D. J. Jacob, P. Suntharalingam, D. B. A. Jones, A. S. Denning, M. E. Nicholls, S. C. Doney, S. Pawson, H. Boesch, B. J. Connor, I. Y. Fung, D. O'Brien, R. J. Salawitch, S. P. Sander, B. Sen, P. Tans, G. C. Toon, P. O. Wennberg, S. C. Wofsy, Y. L. Yung, and R. M. Law, J. Geophys. Res., [Atmos.] **112**(D10), D10314, doi:10.1029/2006JD007659 (2007).
[2]D. Crisp, R. M. Atlas, F. M. Breon, L. R. Brown, J. P. Burrows, P. Ciais, B. J. Connor, S. C. Doney, I. Y. Fung, D. J. Jacob, C. E. Miller, D. O'Brien, S. Pawson, J. T. Randerson, P. Rayner, R. J. Salawitch, S. P. Sander, B. Sen, G. L. Stephens, P. P. Tans, G. C. Toon, P. O. Wennberg, S. C. Wofsy, Y. L. Yung, Z. M. Kuang, B. Chudasama, G. Sprague, B. Weiss, R. Pollock, D. Kenyon, and S. Schroll, in *Trace Constituents in the Troposphere and Lower Stratosphere*, edited by J. P. Burrows, and A. M. Thompson (Pergamon-Elsevier Science Ltd, Kidlington, 2004), Vol. 34, pp. 700–709.
[3]G. D. Spiers, R. T. Menzies, J. Jacob, L. E. Christensen, M. W. Phillips, Y. H. Choi, and E. V. Browell, Appl. Opt. **50**(14), 2098–2111 (2011).
[4]R. A. Toth, L. R. Brown, C. E. Miller, V. M. Devi, and D. C. Benner, J. Quant. Spectrosc. Radiat. Transfer **109**(6), 906–921 (2008).
[5]V. M. Devi, D. C. Benner, L. R. Brown, C. E. Miller, and R. A. Toth, J. Mol. Spectrosc. **245**(1), 52–80 (2007).
[6]V. M. Devi, D. C. Benner, L. R. Brown, C. E. Miller, and R. A. Toth, J. Mol. Spectrosc. **242**(2), 90–117 (2007).
[7]A. Predoi-Cross, W. Liu, C. Holladay, A. V. Unni, I. Schofield, A. R. W. McKellar, and D. Hurtmans, J. Mol. Spectrosc. **246**(1), 98–112 (2007).
[8]T. Hikida, K. M. T. Yamada, M. Fukabori, T. Aoki, and T. Watanabe, J. Mol. Spectrosc. **232**(2), 202–212 (2005).
[9]T. Hikida and K. M. T. Yamada, J. Mol. Spectrosc. **239**(2), 154–159 (2006).
[10]G. Casa, R. Wehr, A. Castrillo, E. Fasci, and L. Gianfrani, J. Chem. Phys. **130**(18), 184306 (2009).
[11]D. A. Long, K. Bielska, D. Lisak, D. K. Havey, M. Okumura, C. E. Miller, and J. T. Hodges, J. Chem. Phys. **135**(6), 064308 (2011).
[12]L. Joly, F. Gibert, B. Grouiez, A. Grossel, B. Parvitte, G. Durry, and V. Zeninari, J. Quant. Spectrosc. Radiat. Transfer **109**(3), 426 (2008).
[13]A. Predoi-Cross, A. R. W. McKellar, D. C. Benner, V. M. Devi, R. Gamache, C. E. Miller, R. A. Toth, and L. R. Brown, Can. J. Phys. **87**(5), 517–535 (2009).
[14]P. Duggan, P. M. Sinclair, A. D. May, and J. R. Drummond, Phys. Rev. A **51**, 218 (1995).
[15]A. S. Pine, J. Quant. Spectrosc. Radiat. Transfer **62**, 397 (1999).
[16]F. Chaussard, R. Saint-Loup, H. Berger, P. Joubert, X. Bruet, J. Bonamy, and D. Robert, J. Chem. Phys. **113**, 4951 (2000).
[17]D. Lisak, G. Rusciano, and A. Sasso, J. Mol. Spectrosc. **227**, 162 (2004).
[18]D. Lisak, G. Rusciano, and A. Sasso, Phys. Rev. A **72**(1), 012503 (2005).
[19]D. Lisak, J. T. Hodges, and R. Ciuryło, Phys. Rev. A **73**, 012507 (2006).
[20]A. Cygan, D. Lisak, S. Wójtewicz, J. Domysławska, J. T. Hodges, R. S. Trawiński, and R. Ciuryło, Phys. Rev. A. **85**, 022508 (2012).
[21]P. L. Varghese and R. K. Hanson, Appl. Opt. **23**(14), 2376–2385 (1984).
[22]F. Schreier, J. Quant. Spectrosc. Radiat. Transfer **48**, 743–762 (1992).
[23]R. H. Dicke, Phys. Rev. **89**(2), 472–473 (1953).
[24]S. G. Rautian and I. I. Sobelman, Sov. Phys. Usp. **9**(5), 701 (1967).

[25]L. Galatry, Phys. Rev. **122**(4), 1218 (1961).
[26]M. Nelkin and A. Ghatak, Phys. Rev. **135**(1A), A4 (1964).
[27]R. Ciuryło, A. S. Pine, and J. Szudy, J. Quant. Spectrosc. Radiat. Transfer **68**(3), 257–271 (2001).
[28]N. H. Ngo, D. Lisak, H. Tran, and J. M. Hartmann, J. Quant. Spectrosc. Radiat. Transfer **129**, 89–100 (2013).
[29]P. W. Anderson, Phys. Rev. **86**, 809 (1952).
[30]J. Szudy and W. E. Baylis, J. Quant. Spectrosc. Radiat. Transfer **15**, 641–668 (1975).
[31]A. Bielski, R. Ciuryło, J. Domysławska, D. Lisak, R. S. Trawiński, and J. Szudy, Phys. Rev. A **62**(3), 032511 (2000).
[32]M. Baranger, Phys. Rev. **111**, 494 (1958).
[33]P. W. Rosenkranz, IEEE Trans. Antennas Propag. **23**, 498–506 (1975).
[34]R. Ciuryło and J. Szudy, Phys. Rev. A **63**, 042714 (2001).
[35]P. R. Berman, J. Quant. Spectrosc. Radiat. Transfer **12**(9), 1331 (1972).
[36]J. Ward, J. Cooper, and E. W. Smith, J. Quant. Spectrosc. Radiat. Transfer **14**(7), 555–590 (1974).
[37]H. M. Pickett, J. Chem. Phys. **73**(12), 6090–6094 (1980).
[38]R. Ciuryło and J. Szudy, J. Quant. Spectrosc. Radiat. Transfer **57**, 411 (1997).
[39]B. Lance, G. Blanquet, J. Walrand, and J. P. Bouanich, J. Mol. Spectrosc. **185**(2), 262–271 (1997).
[40]R. Ciuryło, Phys. Rev. A. **58**(2), 1029–1039 (1998).
[41]D. Priem, F. Rohart, J. M. Colmont, G. Wlodarczak, and J. P. Bouanich, J. Mol. Struct. **517**, 435–454 (2000).
[42]R. Ciuryło, R. Jaworski, J. Jurkowski, A. S. Pine, and J. Szudy, Phys. Rev. A **63**, 032507 (2001).
[43]D. Lisak, A. Cygan, P. Wcisło, and R. Ciuryło, J. Quant. Spectrosc. Radiat. Transfer **151**, 43 (2015).
[44]J. Domysławska, S. Wójtewicz, A. Cygan, K. Bielska, D. Lisak, P. Masłowski, R. S. Trawiński, and R. Ciuryło, J. Chem. Phys. **139**, 194312 (2013).
[45]L. Demeio, S. Green, and L. Monchick, J. Chem. Phys. **102**, 9160 (1995).
[46]A. S. Pine, J. Chem. Phys. **101**, 3444 (1994).
[47]P. Joubert, J. Bonamy, D. Robert, J. Domenech, and D. Bermejo, J. Quant. Spectrosc. Radiat. Transfer **61**, 519 (1999).
[48]W. J. Massman, Atmos. Environ. **32**(6), 1111–1127 (1998).
[49]J. T. Hodges, H. P. Layer, W. W. Miller, and G. E. Scace, Rev. Sci. Instrum. **75**(4), 849–863 (2004).
[50]D. A. Long, A. Cygan, R. D. van Zee, M. Okumura, C. E. Miller, D. Lisak, and J. T. Hodges, Chem. Phys. Lett. **536**, 1–8 (2012).
[51]J. T. Hodges and R. Ciuryło, Rev. Sci. Instrum. **76**, 023112 (2005).
[52]D. Halmer, G. von Basum, P. Hering, and M. Mürtz, Rev. Sci. Instrum. **75**, 2187 (2004).
[53]D. Lisak and J. T. Hodges, Appl. Phys. B **88**(2), 317–325 (2007).
[54]L. S. Rothman, I. E. Gordon, Y. Babikov, A. Barbe, D. C. Benner, P. F. Bernath, M. Birk, L. Bizzocchi, V. Boudon, L. R. Brown, A. Campargue, K. Chance, E. A. Cohen, L. H. Coudert, V. M. Devi, B. J. Drouin, A. Fayt, J. M. Flaud, R. R. Gamache, J. J. Harrison, J. M. Hartmann, C. Hill, J. T. Hodges, D. Jacquemart, A. Jolly, J. Lamouroux, R. J. Le Roy, G. Li, D. A. Long, O. M. Lyulin, C. J. Mackie, S. T. Massie, S. Mikhailenko, H. S. P. Muller, O. V. Naumenko, A. V. Nikitin, J. Orphal, V. Perevalov, A. Perrin, E. R. Polovtseva, C. Richard, M. A. H. Smith, E. Starikova, K. Sung, S. Tashkun, J. Tennyson, G. C. Toon, V. G. Tyuterev, and G. Wagner, J. Quant. Spectrosc. Radiat. Transfer **130**, 4–50 (2013).
[55]D. Priem, J. M. Colmont, F. Rohart, G. Wlodarczak, and R. Gamache, J. Mol. Spectrosc. **204**, 204 (2000).
[56]J. F. D'Eu, B. Lemoine, and F. Rohart, J. Mol. Spectrosc. **212**, 96 (2002).
[57]F. Rohart, G. Wlodarczak, J. M. Colmont, G. Cazzoli, L. Dore, and C. Puzzarini, J. Mol. Spectrosc. **251**, 282 (2008).
[58]D. C. Benner, C. P. Rinsland, V. M. Devi, M. A. H. Smith, and D. Atkins, J. Quant. Spectrosc. Radiat. Transfer **53**(6), 705–721 (1995).
[59]A. S. Pine and R. Ciuryło, J. Mol. Spectrosc. **208**, 180 (2001).
[60]A. S. Pine and T. Gabard, J. Quant. Spectrosc. Radiat. Transfer **66**, 69 (2000).
[61]P. Duggan, P. M. Sinclair, R. Berman, A. D. May, and J. R. Drummond, J. Mol. Spectrosc. **186**(1), 90–98 (1997).
[62]M. D. De Vizia, F. Rohart, A. Castrillo, E. Fasci, L. Moretti, and L. Gianfrani, Phys. Rev. A **83**, 052506 (2011).
[63]D. Lisak, D. K. Havey, and J. T. Hodges, Phys. Rev. A **79**(5), 052507 (2009).
[64]P. Amodio, L. Moretti, A. Castrillo, and L. Gianfrani, J. Chem. Phys. **140**, 044310 (2014).
[65]M. D. De Vizia, A. Castrillo, E. Fasci, P. Amodio, L. Moretti, and L. Gianfrani, Phys. Rev. A **90**, 022503 (2014).
[66]N. H. Ngo, D. Lisak, H. Tran, and J. M. Hartmann, J. Quant. Spectrosc. Radiat. Transfer **134**, 105 (2014).
[67]H. Tran, N. H. Ngo, and J. M. Hartmann, J. Quant. Spectrosc. Radiat. Transfer **129**, 199 (2013).
[68]J. Tennyson, P. F. Bernath, A. Campargue, A. G. Csaszar, L. Daumont, R. R. Gamache, J. T. Hodges, D. Lisak, O. V. Naumenko, L. S. Rothman, H. Tran, N. F. Zobov, J. Buldyreva, C. D. Boone, M. D. De Vizia, L. Gianfrani, J. M. Hartmann, R. McPheat, D. Weidmann, J. Murray, N. H. Ngo, and O. L. Polyansky, "Recommended isolated-line profile for representing high-resolution spectroscopic transitions (IUPAC Technical Report)," Pure Appl. Chem. (in press).
[69]R. A. Toth, C. E. Miller, L. R. Brown, V. M. Devi, and D. C. Benner, J. Mol. Spectrosc. **243**, 43–61 (2007).
[70]R. A. Toth, C. E. Miller, V. M. Devi, D. C. Benner, and L. R. Brown, J. Mol. Spectrosc. **246**(2), 133–157 (2007).